materials

MDPI

Article

A DOPO-Based Compound Containing Aminophenyl Silicone Oil for Reducing Fire Hazards of Polycarbonate

Xiaoqing Song, Wendi Xu, Boyu Cai, Luze Wang, Zhonglin Luo and Biaobing Wang *

Jiangsu Key Laboratory of Environmentally Friendly Polymeric Materials, School of Materials Science and Engineering, Jiangsu Collaborative Innovation Center of Photovoltaic Science and Engineering, Changzhou University, Changzhou 213164, China

* Correspondence: biaobing@cczu.edu.cn; Tel.: +86-0519-8633-0075

Abstract: A novel P/N/Si-containing flame retardant (marked as DASO) was synthesized through an Atherton–Todd reaction between 9,10-dihydro-9-oxa-10-phospha-phenanthrene-10-oxide and aminophenyl silicone oil, and further used for reducing fire hazards of polycarbonate (PC). The chemical structure of DASO was verified via FTIR, ^{1}H, and ^{31}P NMR. Upon the incorporation of 2 wt% DASO, the FRPC composite achieved a high limiting oxygen index (LOI) of 32.2% and a desired UL-94 V-0 rating. In this case, the peak heat release rate (PHRR) and total smoke production (TSP) were reduced by 26% and 44% as compared with the pure PC, respectively. The improved fire safety contributed to the flame retardant roles of DASO in both the condensed phase and gas phase. The presence of DASO promoted the formation of dense and highly graphited char layer in the condensed phase, and released non-combustible gases and phosphorus-containing radicals in the gas phase. Furthermore, the FRPC composites displayed comparable elongation at break but a slightly reduced tensile and impact strength.

Keywords: polycarbonate; P/N/Si-containing flame retardant; fire hazard; mechanical properties

Citation: Song, X.; Xu, W.; Cai, B.; Wang, L.; Luo, Z.; Wang, B. A DOPO-Based Compound Containing Aminophenyl Silicone Oil for Reducing Fire Hazards of Polycarbonate. *Materials* **2023**, *16*, 1449. https://doi.org/10.3390/ma16041449

Academic Editor: Alfonso Maffezzoli

Received: 20 December 2022
Revised: 3 February 2023
Accepted: 7 February 2023
Published: 9 February 2023

1. Introduction

Bisphenol-A polycarbonate (PC) has been widely used in a variety of industrial fields owing to its excellent comprehensive performances, including impact strength, dimensional stability, heat resistance, and transparency [1,2]. Although the PC itself shows a UL-94 V-2 rating for its capability of self-carbonation to a certain degree, it is still far below the stringent requirements of a V-0 rating for harsh applications [3,4]. As we all know, fire accidents bring about a great threat to human security and the environment; it is thus urgent to enhance the fire resistance of PC to expand its application. Over the past decades, a majority of halogenated flame retardants (FRs), although characterized by low cost and better flame retardant effect, have been forbidden for the release of some toxic gases such as halogenated dioxins and dibenzofurans during the combustion. Recently, many efforts have been devoted to preparing halogen-free FRs in order to meet the harsh regulations regarding environmental protection and human health.

Up to date, different types of halogen-free FRs suitable for PC have been reported, such as silicon- [5,6], phosphorus- [7,8], sulfur- [9,10], nitrogen- [11,12], and multi-elements-based compounds [13,14]. However, satisfactory flame retardant efficiency was achieved merely at its high loading level for most halogen-free compounds containing a single FR element, thus generally deteriorating the mechanical properties of the PC matrix. Due to the synergistic effect of the different FR elements, the compounds containing multi-elements display better efficiency for enhancing the fire safety of the PC matrix. Consequently, many works have focused on the synthesis of multi-in-one flame retardants, such as P/N [15,16], P/S [17,18], P/Si [19,20], P/S/N [21,22], etc. Chen et al. [23] prepared PC-based composites blended with phosphazene-triazine bi-group flame retardant (A3); the

PC/A3 composites reached a V-0 rating and 29.3% of LOI value in the case of 13.5% A3 loading level. Yang et al. [24] synthesized a halogen-free FR containing sulfonamide (FRSN), the incorporation of only 0.08 wt% FRSN endowed PC with an LOI value of 33.7% and V-0 rating. According to the report of Hu et al. [25], a novel P/Si-containing FR (P(DOPO-VTES)) was synthesized and adopted to improve the flame retardancy of PC. A maximal LOI value of 32.8% was achieved for PC/5%P(DOPO-VTES) composite, and a V-0 rating was further obtained for PC/5%P(DOPO-VTES)/2 wt% montmorillonite composite.

However, the introduction of additive FRs sometimes deteriorates the mechanical properties of the PC composite due to their poor compatibility, especially in the case of the usage of an anti-dripping agent such as talc and PTFE. Therefore, it is still a challenge to endow the PC matrix with better flame retardancy meanwhile keep almost the mechanical properties. The effect stratagem is to improve the compatibility of the FRs with PC or avoid the usage of an anti-dripping agent. It was well accepted that silicon-based FRs mainly decomposed to form silicon-containing fragments for improving the degree of graphitization of the condensed phase [26–28] and also produced inorganic SiO_2 acting as a protective barrier to keep the internal substrate from further burning. In the present work, a P/N/Si-containing FR (DASO) was synthesized using DOPO and aminophenyl silicone oil as raw materials. Subsequently, the DASO acting as both flame retardant and an anti-dripping agent was blended with PC. As expected, the UL-94 V0 rating was obtained for PC/2 wt% DASO composite accompanied with comparable mechanical properties. Furthermore, the overall properties of the FRPC composites were investigated, and the flame retardant effect on the gas and condensed phase was disclosed.

2. Experimental

2.1. Synthesis of DASO

DASO was prepared through Atherton–Todd reaction between DOPO and APSO (Scheme 1). To a 250 mL three-neck flask equipped with a magnetic stirrer and a reflux condenser, DOPO (0.54 g, 2.5 mmol), APSO (24 g, 2.5 mmol), CH_2Cl_2 (50 mL), and triethylamine (0.25 g, 2.5 mmol) were introduced. Following that, DOPO was dissolved, CCl_4 (0.385 g, 2.5 mmol) was added dropwise under stirring in an ice bath. Subsequently, the mixture was heated to 40 °C and kept the temperature for 12 h. Afterward, triethylamine salt and CH_2Cl_2 were removed by vacuum filtration and rotary evaporation, respectively. The crude product was dissolved in dichloromethane and washed with deionized water several times. Finally, after the removal of dichloromethane by rotary evaporation and vacuum drying at 100 °C for 24 h, it gives a yellow oily liquid (named DASO) with a yield of 91%.

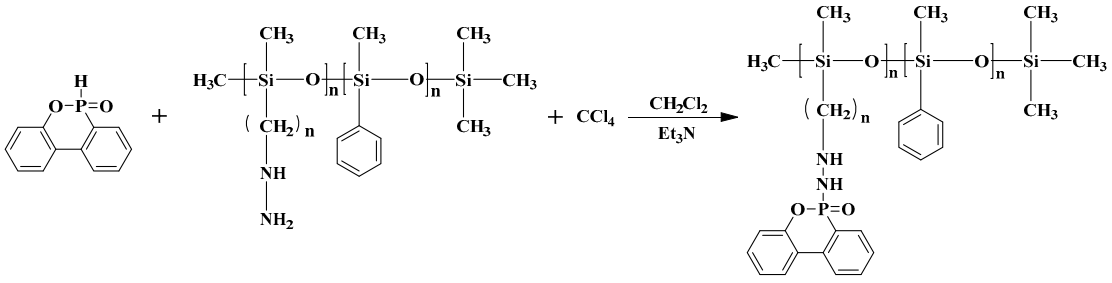

Scheme 1. The synthetic route of DASO.

2.2. Preparation of FRPC Composites

Prior to blending, the PC was vacuum-dried at 100 °C for overnight. The predetermined PC and DASO (Table 1) were blended on an internal mixer (US-70c, Suyan Technology CO., Ltd., Changzhou, China) at 250 °C for 5 min with a rotor speed of 60 r/min. The prepared blends were marked FRPC-X, wherein X denotes the weight percentage of DASO.

Table 1. Formula table of PC and FRPCs.

Sample	PC (wt%)	DASO (wt%)
PC	100	0
FRPC-1	99	1
FRPC-2	98	2

3. Results and Discussion

3.1. Characterization of DASO

The FTIR spectra of APSO, DOPO, and DASO are present in Figure S1. As seen, both APSO and DASO display some typical absorption peaks as follows: 3065 cm^{-1} ($\upsilon_{\varphi\text{-H}}$), 2965 ($\upsilon_{CH3}$) and 2905 cm^{-1} (υ_{CH2}), 1260 and 804 cm^{-1} ($\upsilon_{Si\text{-C}}$), 1093 and 1023 cm^{-1} ($\upsilon_{Si\text{-O-Si}}$). Moreover, the peak at 2437 cm^{-1} ascribed to $\upsilon_{P\text{-H}}$ [29] disappears, while some characteristic absorption peaks at 1214 ($\upsilon_{P\text{-O-C}}$) and 932 cm^{-1} ($\upsilon_{P\text{-N}}$) are easily visible in the spectrum of DASO. It indicates that the DASO is synthesized successfully.

Regarding the ^{1}H NMR (Figure S2a), the signals at 7–8 ppm are assigned to protons (c + e + f + h) of the benzene ring and -NH, and the one at 5.21 ppm ascribes to the proton (g) of -NH connected with CH_2. The protons (a and b) from CH_3 appear at 0.05 and 0.56 ppm, and the signal at 2.46 ppm is ascribed to proton (d) from CH_2. As shown in ^{31}P NMR (Figure S2b,c), the chemical shifts at 14.51 and 15.72 ppm for DOPO merge into a single signal at 7.06 ppm for DASO, which might be triggered by the steric hindrance of phosphaphenanthrene group [30].

As presented in the TGA and DTG curves of DASO (Figure S3), the DASO displays a three-step degradation behavior with $T_{5\%}$ (5% mass loss temperature) of 293 °C, indicating the DASO fully meets the processing temperature of PC. The first stage originates from the breakage of P-N and P-C bonds, the second one with T_{max} (maximum decomposition temperature) of 467 °C is attributed to the breakage of the N-H and C-N bonds, and the last one with T_{max} of 580 °C includes the rapture of Si-C and Si-O-Si in the main chain.

3.2. Thermal Stability of PC and FRPCs

The thermal stability of the samples was assessed in terms of TGA, and the relative TGA and DTG curves are depicted in Figure 1, and Table 2 lists the values of $T_{5\%}$, T_{max}, R_{max} (maximum decomposition rate), and CY_{800} (char yields at 800 °C). It is found that both PC and FRCPs display a one-step thermal decomposition process under a nitrogen atmosphere, revealing that the incorporation of DASO exerts no obvious changes on the thermal decomposition process of PC. However, the FRPCs present lower values of $T_{5\%}$ and T_{max} than the pure PC, which might be attributed to the fact that the DASO with less stable P-C and P-N bonds has a catalytic effect on the degradation of PC. Moreover, the introduction of DASO results in a reduced R_{max} but an enhanced CY_{800}. For instance, the R_{max} is reduced from 33.4%/min for pure PC to 15.5%/min for FRPC-2; conversely, the CY_{800} is increased from 18.4 to 19.6%. It shows that the presence of DASO can catalyze the char-forming to impede the further thermal degradation of the PC matrix, thus exerting FR's role on the condensed phase. Unlike a single-stage decomposition under a nitrogen atmosphere, three-stage decomposition behaviors occur under an air atmosphere. It indicates that the thermal degradation kinetics become much more complicated due to thermal oxidization.

Table 2. Thermal parameters for PC and FRPCs.

Specimen	Nitrogen				Air				
	$T_{5\%}$ (°C)	T_{max} (°C)	R_{max} (%/min)	CY_{800} (wt%)	$T_{5\%}$ (°C)	T_{max1} (°C)	T_{max2} (°C)	T_{max3} (°C)	CY_{800} (wt%)
PC	507	549	33.4	18.4	474	481	522	593	0.18
FRPC-1	488	537	19.2	19.2	469	471	520	579	0.41
FRPC-2	486	523	15.5	19.6	459	475	517	569	0.55

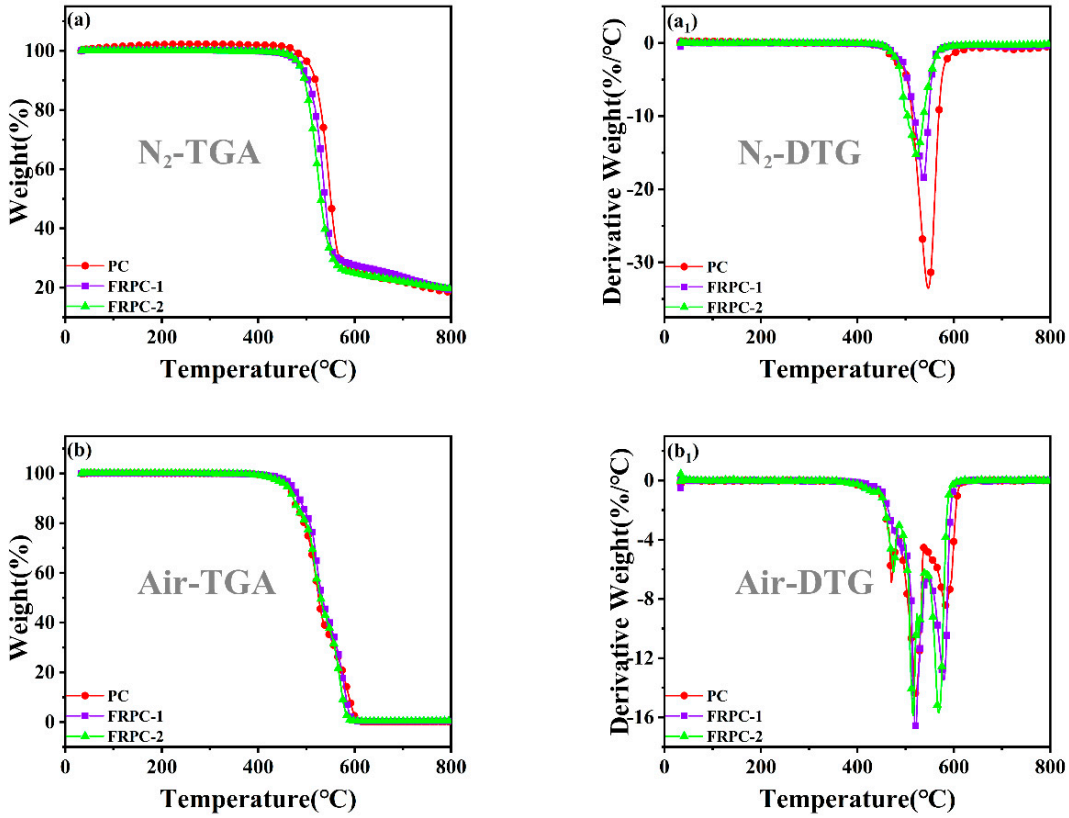

Figure 1. TGA and DTG curves of PC and FRPCs under N_2 (**a**,**a**$_1$) and air (**b**,**b**$_1$).

3.3. Flame Retardancy Analysis

Figure 2 illustrates the UL-94 rating and LOI values of the samples. As expected, flame retardancy improves steadily upon the increasing DASO contents. For example, the LOI value is increased from 25% for pure PC with a V-2 rating to 32.2% for FRPC-2 with a V-0 rating. Moreover, few char residues are produced during the LOI testing of pure PC; in contrast, much more compact char residues that can withstand the pressure of 20 g poise are left upon the incorporation of DASO.

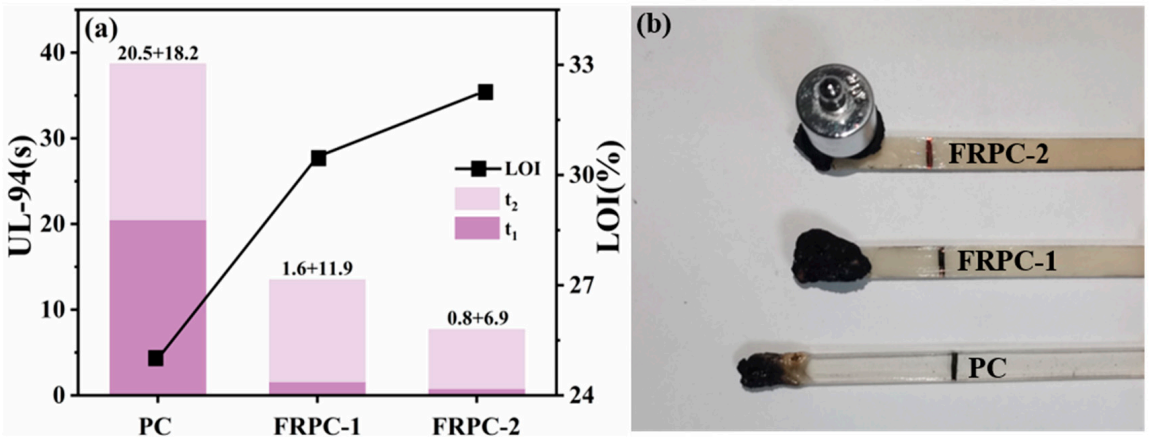

Figure 2. Flame retardancy (**a**) and digital photographs of char residues (**b**).

3.4. Cone Calorimeter Tests

Figure 3 shows the curves of heat release rate (HRR), total heat release (THR), smoke production rate (SPR), and total smoke production (TSP), and Table 3 summarizes some specific parameters.

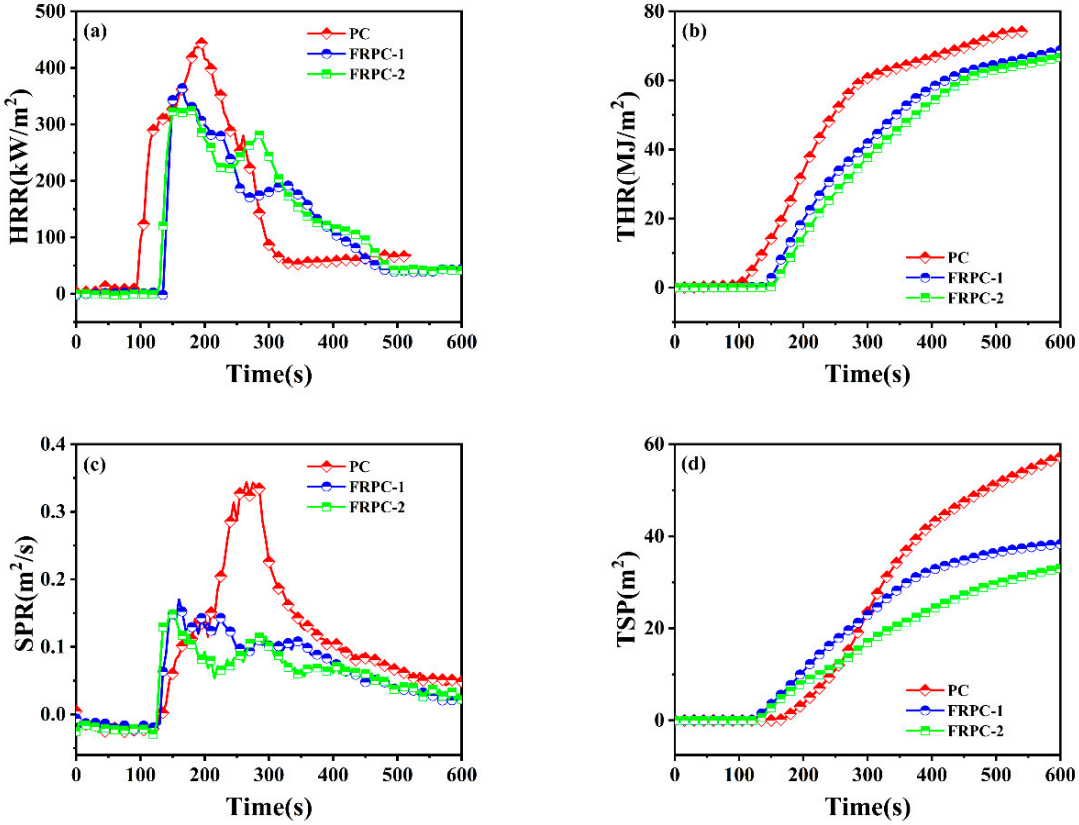

Figure 3. HRR (**a**), THR (**b**), SPR (**c**) and TSP (**d**) curves obtained from CCT.

Table 3. Cone calorimeter parameters of PC and FRPCs.

Sample	PC	FRPC-1	FRPC-2
TTI (s)	150	130	123
PHRR (kW/m^2)	443.5	364.0	326.1
t-PHRR (s)	195	165	160
THR (MJ/m^2)	74.2	72.9	70.2
TSP (m^2)	63.4	39.6	35.4
PSPR	0.34	0.17	0.15
av-COY (kg/kg)	0.10	0.12	0.13
av-CO_2Y (kg/kg)	1.73	1.74	1.68
av-EHC (MJ/kg)	24.9	22.8	20.4
Char residue(%)	13.5	13.6	13.9
FIGRA (kW/m^2·s)	2.27	2.21	2.04

As seen, the time to ignition (TTI) shortens steadily with the increasing DASO content, for example, 150 s for pure PC > 130 s for FRPC-1 > 127 s for FRPC-2. The shortened TTI is mainly due to the earlier decomposition of DASO.

Generally, the THR and peak of HRR (PHRR) are valued as crucial parameters to reflect the combustion intensity. In comparison with THR of 74.2 MJ/m^2 and PHRR of 443.5 kW/m^2 for pure PC, these values reduce steadily with the incorporation of DASO. Especially, the minimum values, including 70.2 MJ/m^2 of THR and 326.1 kW/m^2 of PHRR, are achieved for FRPC-2. It demonstrates that the presence of DASO plays inhibiting function on the heat release during combustion. Likewise, toxic smoke is also considered a harmful factor in a real fire [31]. As shown in Figure 3c and Table 3, both SPR and TSP values reduce obviously with the loading of DASO. Particularly, FRPC-2 composite gives the lowest TSP of 35.4 m^2 and PSPR (peak of SPR) of 0.15 m^2/s, with a reduction of 44.2% and 55.9% by comparison with pristine PC, respectively. It reveals that DASO also has better smoke suppression. Additionally, the fire growth rate index (FIGRA = PHRR/T_{PHRR})

is adopted to assess underlying fire spread or growth hazards during burning. As seen in Table 3, the FRPC-2 displays the lowest FIGRA value (2.04 kW/m^2·s) among all samples, reflecting that fire safety is improved with the introduction of DASO.

The value of av-EHC (HRR/MLR) is often used to characterize the burning degree of volatiles in the gas phase. As seen, the av-EHC values offer a downward trend in the following order of PC (24.9 MJ/kg) > FRPC-1 (22.8 MJ/kg) > FRPC-2 (20.4 MJ/kg), demonstrating that DASO decreases the flammability of PC markedly. Additionally, PC/DASO composites give greater av-COY/av-CO_2Y values (0.069 for FRPC-1 and 0.077 for FRPC-2) than that (0.0578) of the pure PC, which reveals that the DASO plays FR roles on gas phase which causing the occurrence of more serious incomplete combustion.

3.5. Characterization of Char Residue

The digital and SEM images of char residues are present in Figure 4. As seen, the pristine PC leaves intumescent char residues with many holes on the surface, which provides the channel for the transfer of heat and mass. In comparison, a smooth and continuous surface, although a tiny crack, still exists for FRPC-1 composite. With the DASO content up to 2 wt%, comparatively, char residue gives an expansion height of ~8.4 cm and becomes more continuous and smoother, which keeps transmission of combustibles and heat from the external surface to the inner matrix [32].

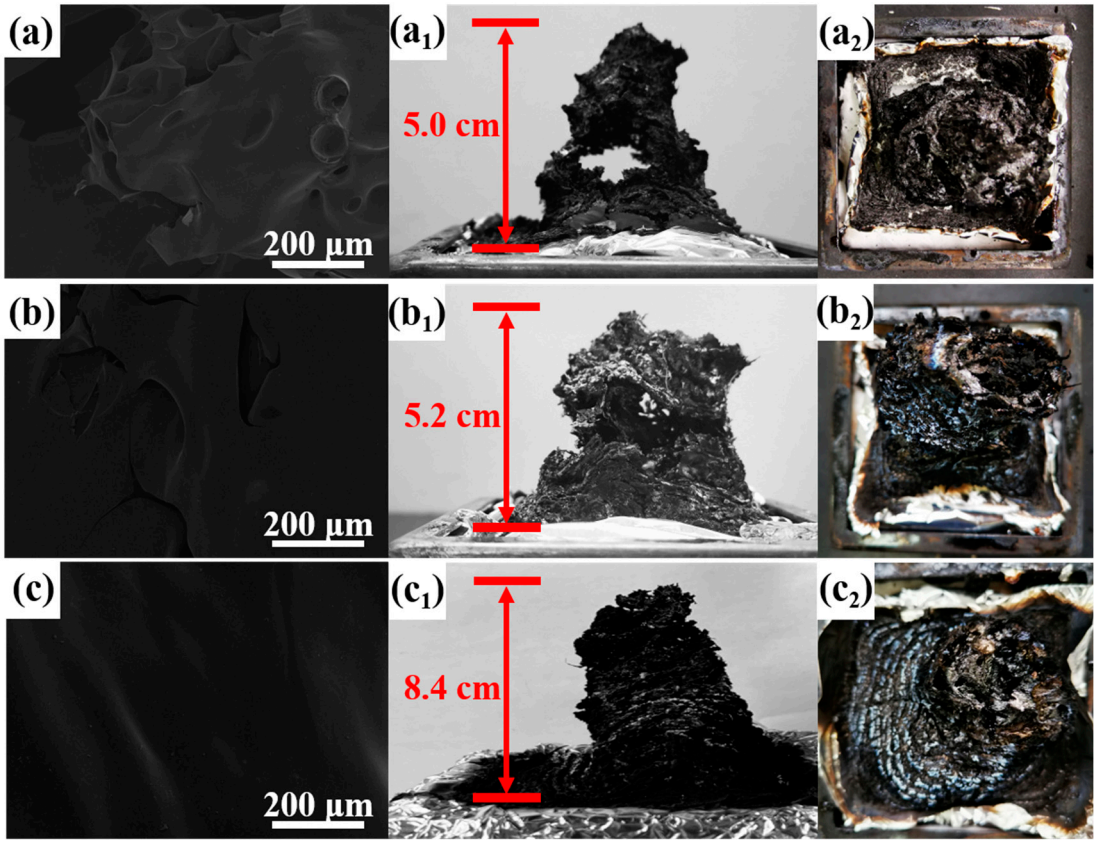

Figure 4. SEM (×200) and Digital images of PC (**a**), FRPC-1 (**b**) and FRPC-2 (**c**); Subscript 1, 2 represent the side and top surface.

As seen in Raman spectra of char residues (Figure S4), two sharp peaks appear at 1360 cm^{-1} (D band) and 1600 cm^{-1} (G band), which are assigned to the disordered carbon impurities (or defects) and 2D hexagonal graphitic lattice, respectively [33,34]. Normally, a lower area ratio (A_D/A_G) of the two peaks reveals a higher graphitization degree. It is found that the A_D/A_G value is decreased from 2.92 for pure PC to 2.41 for FRPC-1 and

2.26 for FRPC-2, revealing that the DASO has a catalytic effect on the graphitization of the char residues.

Figure 5 shows the XPS survey spectra of pure PC and FRPC-2, and the resultant elemental content is listed in Table 4. It is obvious that FRPC-2 contains a small amount of P, Si, and N elements besides C and O elements in the pure PC, indicating that the three flame retardant elements play roles in the condensed phase. In the C1s spectra (Figure 5b), the binding energy peaks at 283.4~283.5 and 284.4~285.1 eV are assigned to C-C/C-H and C-O, respectively. In addition, a new peak at 287.2 eV belongs to C=O for FRPC-2. The O1s spectra (Figure 5c) show that the binding energy peaks located at 531.3~531.5 eV and 532.1~532.8 eV correspond to O-C and C=O, respectively. The peak intensity ratio of C=O/C-O is significantly reduced, indicating that substances with C=O basically overflow into the gas phase, while C-O (ethers and cross-linked structures) remain in the char residues [35]. Regarding the Si2p spectra (Figure 5d), the binding energy peak at ~101.0, ~102.0, and ~103.8 eV are attributed to the bonding states of Si-C, Si-O-C, and Si-O-Si, respectively. It indicates that DASO is thermally decomposed to produce silicon-containing fragments during combustion.

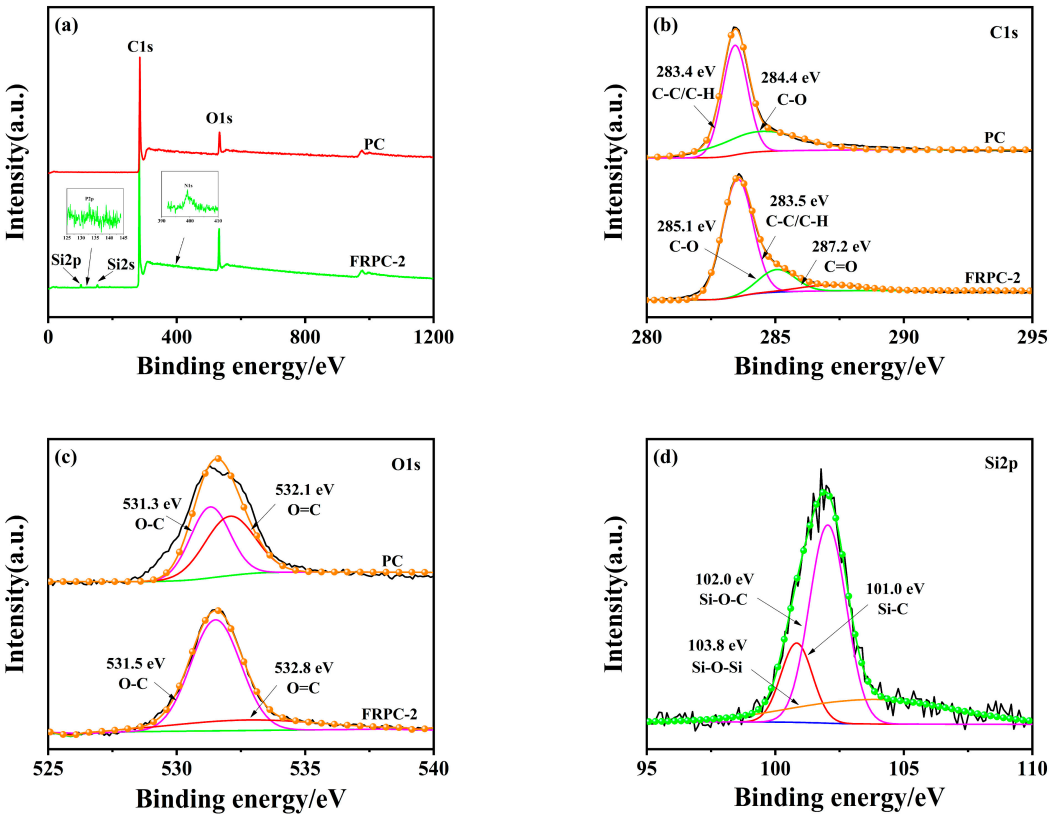

Figure 5. XPS survey spectra (**a**), C1s (**b**) and O1s (**c**) of PC and FRPC-2; Si2p (**d**) spectra of FRPC-2.

Table 4. The elemental contents of the residues of PC and FRPC-2 after CCT.

Sample	C (At%)	O (At%)	Si (At%)	N(At%)	P (At%)
PC	89.80	10.20	0	0	0
FRPC-2	83.65	12.64	2.20	1.25	0.26

3.6. TGA-FTIR Analysis of Gaseous Products

The pyrolysis gases of neat PC and FRPCs at different temperatures were analyzed via TGA-FTIR spectra in order to understand the flame-retardant roles of DASO in the gas phase. As shown in Figure 6a–c, some common gases are produced for all specimens, including H_2O (3658 cm^{-1}), hydrocarbons (2800–3100 cm^{-1}), CO_2 (2300–2400 cm^{-1}), CO

(2080–2190 cm^{-1}), phenyl compounds (1514 cm^{-1}), aromatic ethers (1236 cm^{-1}), and phenol derivatives (1174 cm^{-1}). It is also found that two new peaks at 1258 cm^{-1} and 1068 cm^{-1} occur in FTIR spectra of FRPCs, which belong to P=O and P-O-C [36,37], respectively. The nonflammable gases (H_2O and CO_2) can act as diluting agents for oxygen and combustible volatiles and work synergistically with a small amount of phosphorus-containing fragments as radical scavengers to exert flame-retardant roles in the gas phase [38,39]. Additionally, the 3D real-time evolution TG-FTIR images (Figure 6a_1–c_1) of gaseous products show that the absorbance intensity tends to reduce visibly with the incorporation of DASO. Specifically, Figure S5 shows the change of absorbance intensity of four typical flammable gases (CH_4, phenyl, ether, and C-OH compounds) with time. As seen, the absorbance intensity of flammable volatiles decreases significantly during the decomposition of FRPC composites. It indicates that DASO can suppress the production of flammable volatiles, thus playing the flame retardant role in the gas phase.

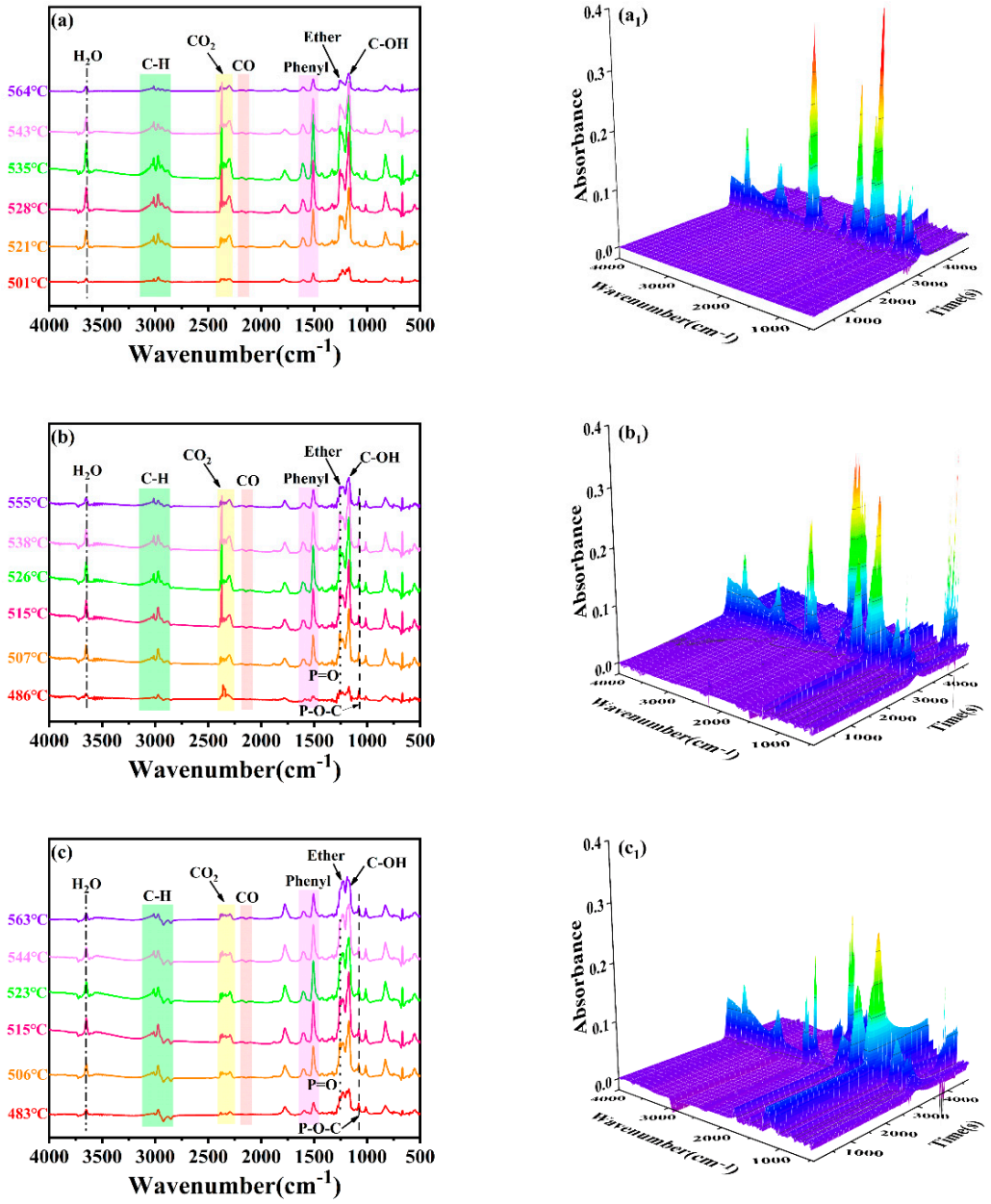

Figure 6. FTIR spectra of gaseous products at various temperatures under nitrogen and 3D images of PC (**a**,**a**$_1$), FRPC-1 (**b**,**b**$_1$), and FRPC-2 (**c**,**c**$_1$).

3.7. Possible Flame Retardant Mechanism

Taking the described-above flame retardant role of DASO in both gas and condensed phase into consideration, a possible flame retardant mechanism is proposed and illustrated in Scheme 2. With respect to the gas phase, nonflammable gases (H_2O and CO_2) dilute oxygen and flammable volatiles and work synergistically with phosphorus-containing radicals (·PO and ·PO_2) as radical scavengers to capture the highly active radicals (H· and HO·) during the combustion process, further combustion is consequently slowed down. As to the condensed phase, the phosphorus- and silicone-containing fragments promote and participate in the formation of a dense and highly graphited char layer with Si-O-C and phosphorus-rich structure during the combustion, which acts as a physical barrier to inhibit the transfer of heat and flammable volatiles.

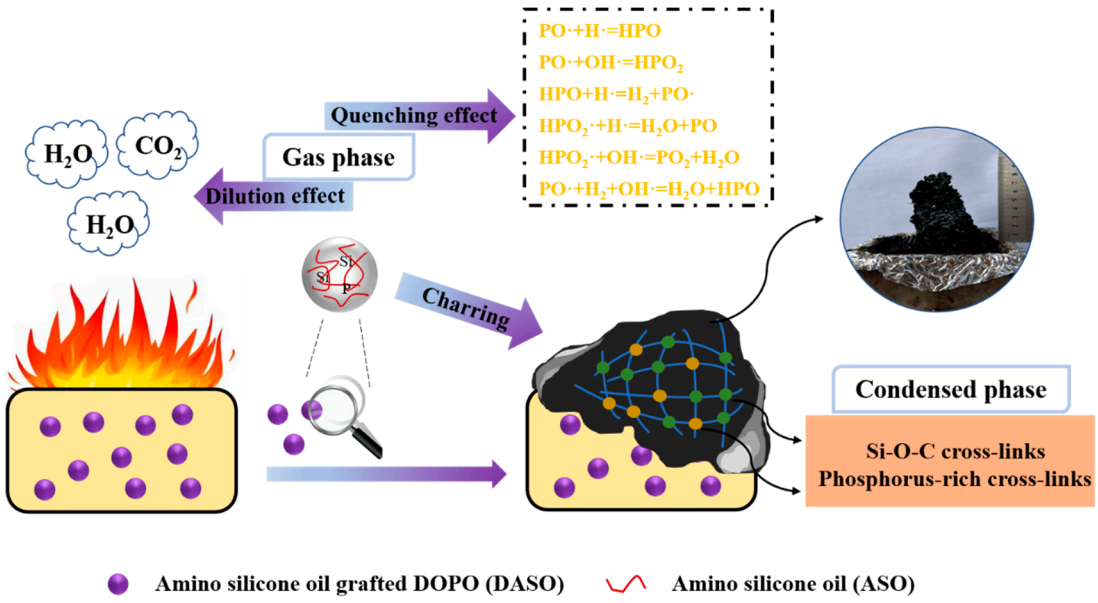

Scheme 2. Flame-retardant mechanism of FRPC composites.

3.8. Mechanical Properties

The influence of DASO on mechanical performances was evaluated according to tensile and impact testing, and the specific data are summarized in Table 5. By comparison with the pristine PC presenting tensile strength of 60.3 MPa, elongation at break of 87.6%, and impact strength of 68.9 kJ/m^2, the FRPC composites keep almost the same elongation at break whilst their tensile and impact strength are reduced. For instance, the FRPC-2 presents tensile strength of 54.3 MPa and 57.2 kJ/m^2, with a reduction of 10.0% and 17.0% compared to the pure PC, respectively. As we know, the mechanical performances of the composite correlate with the microstructure of the multiphase. As seen in Figure 7, all specimens show impact-fractured rough surfaces with ductile fracture characteristics. However, it is noted that FRPCs present obvious droplets, which act as stress concentration points, and the mechanical properties are reduced accordingly.

Table 5. Mechanical performances of PC and its FRPCs.

Sample	PC	FRPC-1	FRPC-2
Tensile strength (MPa)	60.3 ± 0.8	57.6 ± 1.4	54.3 ± 0.5
Elongation at break (%)	87.6 ± 2.9	85.9 ± 4.9	83.0 ± 5.3
Impact strength (KJ/m^2)	68.9 ± 1.2	60.3 ± 0.9	57.2 ± 0.6

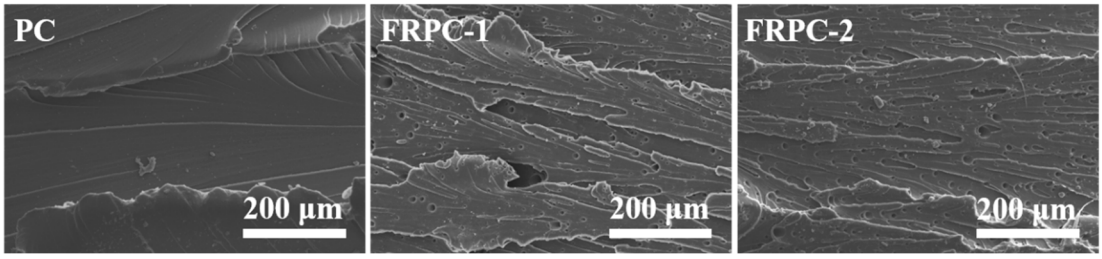

Figure 7. SEM images of the impact-fractured surface of PC and its FRPCs.

4. Conclusions

In summary, a novel Si/N/P-containing flame retardant (DASO) was synthesized through an Atherton–Todd reaction between DOPO and aminophenyl silicone oil, and its chemical structure was confirmed in terms of FTIR, ^{1}H NMR, and ^{31}P NMR. Furthermore, the DASO was adopted to improve the fire safety of PC. A V-0 rating and a high LOI of 32.2% were obtained for FRPC-2. Meanwhile, its PHRR and TSP were reduced by 26% and 44% by comparison with neat PC, respectively. The comprehensive analysis of char residues and pyrolysis gases showed that DASO played a synergistic flame retardant effect in both the gas and condensed phase. In the gas phase, it included the quenching effect of the free radicals (·PO and ·PO_2) and the diluting effect of the nonflammable gases (H_2O and CO_2). Regarding the condensed phase, the phosphorus- and silicone-containing compounds produced from the degradation of DASO promoted and participated in the formation of a dense and highly graphited char layer, which acted as a physical barrier to inhibit the transfer of heat and flammable volatiles. Furthermore, the FRPCs keep almost the same elongation at break whilst their tensile and impact strength are reduced slightly.

Supplementary Materials: The following supporting information can be downloaded at: https://www.mdpi.com/article/10.3390/ma16041449/s1, Figure S1: FTIR spectra of DOPO, APSO, and DASO.; Figure S2: 1H NMR spectra of DASO (a), 31P NMR spectra of DOPO (b) and DASO (c).; Figure S3: TGA and DTG curves of DASO.; Figure S4: Raman spectra of char residues for PC (a), FRPC-1 (b), and FRPC-2 (c).; Figure S5: Absorption intensities of CH4 (a), phenyl (b), ether (c), and C-OH (d) versus time in the thermal degradation for PC and FRPCs.

Author Contributions: Methodology, B.C.; Formal analysis, L.W.; Investigation, X.S.; Resources, W.X.; Writing—original draft, X.S.; Writing—review & editing, Z.L.; Supervision, B.W.; Project administration, B.W. All authors have read and agreed to the published version of the manuscript.

Funding: This research received no external funding.

Institutional Review Board Statement: Not applicable.

Informed Consent Statement: Not applicable.

Data Availability Statement: Not applicable.

Conflicts of Interest: The authors declare no conflict of interest.

References

1. Bagotia, N.; Choudhary, V.; Sharma, D.K. Synergistic effect of graphene/multiwalled carbon nanotube hybrid fillers on mechanical, electrical and EMI shielding properties of polycarbonate/ethylene methyl acrylate nanocomposites. *Compos. Part B Eng.* **2019**, *159*, 378–388. [CrossRef]
2. Liang, C.; Liu, S.; Wirasaputra, A.; Zhao, J.; Fu, Y. Light difusing and fame-retardant polycarbonate modifed by highly efcient and multifunctional organosilica microspheres. *J. Therm. Anal. Calorim.* **2021**, *146*, 2423–2433. [CrossRef]
3. Shi, L.; Chew, M.Y. A review of fire processes modeling of combustible materials under external heat flux. *Fuel* **2013**, *106*, 30–50. [CrossRef]
4. Wang, J.B.; Xin, Z. Flame Retardancy, Thermal, Rheological, and Mechanical Properties of Polycarbonate/Polysilsesquioxane System. *J. Appl. Polym. Sci.* **2010**, *115*, 330–337. [CrossRef]
5. Li, Z.Q.; Yang, R.J. Flame retardancy, thermal and mechanical properties of sulfonate-containing polyhedral oligomeric silsesquioxane (S-POSS)/polycarbonate composite. *Polym. Degrad. Stabil.* **2015**, *116*, 81–87. [CrossRef]

6. Wei, Y.-X.; Deng, C.; Zhao, Z.-Y.; Wang, Y.-Z. A novel organic-inorganic hybrid SiO_2@DPP for the fire retardance of polycarbonate. *Polym. Degrad. Stabil.* **2018**, *154*, 177–185. [CrossRef]
7. Feng, J.; Hao, J.; Du, J.; Yang, R. Flame retardancy and thermal properties of solid bisphenol A bis(diphenyl phosphate) combined with montmorillonite in polycarbonate. *Polym. Degrad. Stabil.* **2010**, *95*, 2041–2048. [CrossRef]
8. Zhou, X.; Qiu, S.; Mu, X.; Zhou, M.; Cai, W.; Song, L.; Xing, W.; Hu, Y. Polyphosphazenes-based flame retardants: A review. *Compos. B Eng.* **2020**, *202*, 108397. [CrossRef]
9. Xia, L.; Li, F.; Shentu, B.; Weng, Z. Thermal Degradation Behavior and Flame Retardancy of Polycarbonate Containing Poly[(phenylsilsesquioxane)-co-(dimethylsio-ane)] and Potassium Diphenyl Sulfonate. *J. Macromol. Sci. Part B Phys.* **2015**, *52*, 310–318. [CrossRef]
10. Sai, T.; Ran, S.; Huo, S.; Guo, Z.; Song, P.; Fang, Z. Sulfonated Block Ionomers Enable Transparent, Fire-Resistant, Tough yet Strong Polycarbonate. *Chem. Eng. J.* **2022**, *433*, 133264. [CrossRef]
11. Zhao, W.; Li, B.; Xu, M.; Yang, K.; Lin, L. Novel intumescent flame retardants: Synthesis and application in polycarbonate. *Fire Mater.* **2013**, *37*, 530–546. [CrossRef]
12. Nguyen, C.; Kim, J. Thermal stabilities and flame retardancies of nitrogen-phosphorus flame retardants based on bisphosphoramidates. *Polym. Degrad. Stabil.* **2008**, *93*, 1037–1043. [CrossRef]
13. Qian, Z.; Zou, B.; Xiao, Y.; Qiu, S.; Xu, Z.; Yang, Y.; Jiang, G.; Zhang, Z.; Song, L.; Hu, Y. Targeted modification of black phosphorus by MIL-53(Al) inspired by "Cannikin's Law" to achieve high thermal stability of flame retardant polycarbonate at ultra-low additions. *Compos. B Eng.* **2022**, *238*, 109943. [CrossRef]
14. Nabipour, H.; Wang, X.; Song, L.; Hu, Y. Metal-organic frameworks for flame retardant polymers application: A critical review. *Compos. Part A Appl. Sci. Manuf.* **2020**, *139*, 106113. [CrossRef]
15. Qin, Y.; Li, M.; Huang, T.; Shen, C.; Gao, S. A study on the modification of polypropylene by a star-shaped intumescent flame retardant containing phosphorus and nitrogen. *Polym. Degrad. Stabil.* **2020**, *195*, 109801. [CrossRef]
16. Zheng, T.; Wang, W.; Liu, Y. A novel phosphorus-nitrogen flame retardant for improving the flame retardancy of polyamide 6: Preparation, properties, and flame retardancy mechanism. *Polym. Adv. Technol.* **2021**, *32*, 2508–2516. [CrossRef]
17. Zhao, W.; Li, B.; Xu, M.; Zhang, L.; Liu, F.; Guan, L. Synthesis of a Novel Flame Retardant Containing Phosphorus and Sulfur and Its Application in Polycarbonate. *Polym. Eng. Sci.* **2012**, *52*, 2327–2335. [CrossRef]
18. Xu, M.; Zhao, W.; Li, B.; Yang, K.; Lin, L. Synthesis of a phosphorus and sulfur-containing aromatic diamine curing agent and its application in flame retarded epoxy resins. *Fire Mater.* **2015**, *39*, 518–532. [CrossRef]
19. Niu, Q.; Yue, X.; Guo, Z.; Yan, H.; Fang, Z.; Li, J. Flame retardant bamboo fiber reinforced polylactic acid composites regulated by interfacial phosphorus-silicon aerogel. *Polymer* **2022**, *252*, 124961. [CrossRef]
20. Luo, X.; Hu, H.; Ma, J.; Huang, Y.; Yang, J. Synthesis and characterization of dicyclic silicon-/phosphorus-grafted alumina and its application in improving flame retardancy of epoxy resin. *J. Appl. Polym. Sci.* **2021**, *138*, 49854. [CrossRef]
21. Jiang, G.; Xiao, Y.; Qian, Z.; Yang, Y.; Jia, P.; Song, L.; Hu, Y.; Ma, C.; Gui, Z. A novel phosphorus-, nitrogen- and sulfur-containing macromolecule flame retardant for constructing high-performance epoxy resin composites. *Chem. Eng. J.* **2022**, *451*, 137823. [CrossRef]
22. Li, W.; Dou, Y.; Li, X.; Fang, S.; Li, J.; Li, Q. A Highly Effective, UV-Curable, Intumescent, Flame-Retardant Coating Containing Phosphorus, Nitrogen, and Sulfur, Based on Thiol-Ene Click Reaction. *Materials* **2022**, *15*, 3358. [CrossRef] [PubMed]
23. Chen, Y.J.; Wu, X.D.; Qian, L.J. Flame-retardant behavior and protective layer effect of phosphazene-triazine bi-group flame retardant on polycarbonate. *J. Appl. Polym. Sci.* **2020**, *137*, 49523. [CrossRef]
24. Yang, H.; Yue, H.; Zhao, X.; Song, M.; Guo, J.; Cui, Y.; Fernández-Blázquez, J.P.; Wang, D.-Y. Polycarbonate/Sulfonamide Composites with Ultralow Contents of Halogen-Free Flame Retardant and Desirable Compatibility. *Materials* **2020**, *13*, 3656. [CrossRef] [PubMed]
25. Hu, Z.; Chen, L.; Zhao, B.; Luo, Y.; Wang, D.-Y.; Wang, Y.-Z. A novel efficient halogen-free flame retardant system for polycarbonate. *Polym. Degrad. Stabil.* **2011**, *96*, 320–327. [CrossRef]
26. Wang, Z.; Yonggang, L.; Huijuan, M.; Wenpeng, S.; Tao, L.; Cuifen, L.; Junqi, N.; Guichun, Y.; Zuxing, C. Novel phosphorus-nitrogen-silicon copolymers with double-decker silsesquioxane in the main chain and their flame retardancy application in PC/ABS. *Fire Mater.* **2018**, *42*, 946–957. [CrossRef]
27. Wei, Y.-X.; Deng, C.; Wei, W.-C.; Chen, H.; Wang, Y.-Z. Hybrid Nanorods Comprised of Titanium, Silicon, and Organophosphorus as Additives for Flame-Retardant Polycarbonate. *ACS. Appl. Nano. Mater.* **2019**, *2*, 4859–4868. [CrossRef]
28. Wan, Y.; Yu, S.; Jiang, S.; Pei, Q.; Xu, S.; Cao, W.; Liu, X.; Lan, Y. Microscopic pyrolysis mechanism on the octyphenylsiloxane flame retarded polycarbonate by reactive molecular dynamics. *J. Anal. Appl. Pyrol.* **2021**, *158*, 105274. [CrossRef]
29. Wang, P.; Yang, F.; Li, L.; Cai, Z. Flame retardancy and mechanical properties of epoxy thermosets modified with a novel DOPO-based oligomer. *Polym. Degrad. Stabil.* **2016**, *129*, 156–167. [CrossRef]
30. Yang, Y.; Chen, W.; Li, Z.; Huang, G.; Wu, G. Efficient flame retardancy, good thermal stability, mechanical enhancement, and transparency of DOPO-conjugated structure compound on epoxy resin. *Chem. Eng. J.* **2022**, *450*, 138424. [CrossRef]
31. Yang, R.; Gu, G.; Tang, C.; Miao, Z.; Cao, H.; Zou, G.; Li, J. Super-tough and flame-retardant poly(lactic acid)materials using a phosphorus-containing malic acid-based copolyester by reactive blending. *Polym. Degrad. Stabil.* **2022**, *198*, 109889. [CrossRef]
32. Zhu, Y.; Yu, R.; Wang, S.; Xing, H.; Qiu, J.; Liu, J.; Tang, T. Unexpected core-shell char from polycarbonate/polyborosiloxane composites and its application in improving flame retardancy. *Chem. Eng. J.* **2022**, *446*, 136742. [CrossRef]

33. Attia, N.F.; Park, J.; Oh, H. Facile tool for green synthesis of graphene sheets and their smart freestanding UV protective film. *Appl. Surf. Sci.* **2018**, *458*, 425–430. [CrossRef]
34. Wu, X.; Qin, Z.; Zhang, W.; Yang, R. KCl nanoparticles-loaded octaphenylsilsesquioxane as an efficient flame retardant for polycarbonate. *React. Funct. Polym.* **2022**, *177*, 105284. [CrossRef]
35. Sai, T.; Su, Y.; Shen, H.; Ran, S.; Huo, S.; Guo, Z.; Fang, Z. Fabrication and Mechanism Study of Cerium-Based P, N-Containing Complexes for Reducing Fire Hazards of Polycarbonate with Superior Thermostability and Toughness. *ACS Appl. Mater. Interfaces* **2021**, *13*, 30061–30075. [CrossRef]
36. Weil, E.D.; Levchik, S. A review of current flame retardant systems for epoxy resins. *J. Fire Sci.* **2004**, *22*, 25–40. [CrossRef]
37. Qian, L.-J.; Ye, L.-J.; Xu, G.-Z.; Liu, J.; Guo, J.-Q. The non-halogen flame retardant epoxy resin based on a novel compound with phosphaphenanthrene and cyclotriphosphazene double functional groups. *Polym. Degrad. Stabil.* **2011**, *96*, 1118–1124. [CrossRef]
38. Sai, T.; Ran, S.; Guo, Z.; Yan, H.; Zhang, Y.; Wang, H.; Song, P.; Fang, Z. Transparent, highly thermostable and flame retardant polycarbonate enabled by rod-like phosphorous-containing metal complex aggregates. *Chem. Eng. J.* **2021**, *409*, 128223. [CrossRef]
39. Wang, H.; Li, S.; Zhu, Z.; Yin, X.; Wang, L.; Weng, Y.; Wang, X. A novel DOPO-based flame retardant containing benzimidazolone structure with high charring ability towards low flammability and smoke epoxy resins. *Polym. Degrad. Stabil.* **2021**, *183*, 109426. [CrossRef]